Experimental observation of three-dimensional non-paraxial accelerating beams

L. LI,[1,3] **Y. JIANG,**[1,3] **P. JIANG,**[1] **X. LI,**[1] **Y. QIU,**[1] **P. JIA,**[1] **Z. PI,**[1] **Y. HU,**[1,*] **Z. CHEN,**[1,2] **AND J. XU**[1]

[1]*The MOE Key Laboratory of Weak-Light Nonlinear Photonics, TEDA Applied Physics Institute and School of Physics, Nankai University, Tianjin 300457, China*
[2]*Department of Physics and Astronomy, San Francisco State University, San Francisco, CA 94132, USA*
[3]*These authors contribute equally to this work*
*yihu@nankai.edu.cn

Abstract: We experimentally realize three-dimensional non-paraxial accelerating beams associated with different coordinate systems. They are obtained by Fourier transforming a phase-modulated wave front in an aberration-compensated system. The phase pattern is encoded to include the phase and amplitude modulation for the accelerating beams with additional correction phase for the aberration compensation. These beams propagate along a circular trajectory, but they exhibit rather complex intensity patterns corresponding to the shape-invariant solutions in parabolic, prolate spheroidal and oblate spheroidal coordinate systems.

1. Introduction

Self-accelerating wave-packets were firstly proposed in quantum mechanics in 1979 [1]. This kind of wave-packets manifests counterintuitively an acceleration in free space without any external potential. Realization of ideal self-accelerating wave-packets faces difficulties in the experiment as they carry infinite energy. In 2007, the concept of self-acceleration was revisited in optics based on a mathematical similarity between the paraxial beam propagation equation and the Schrödinger equation [2]. In particular, finite-energy accelerating beams, namely Airy beams, were produced experimentally via a proper apodization [3]. Since then, these beams as well as their temporal counterparts have received a great deal of attention triggered by their intriguing properties including self-acceleration, non-diffraction and self-healing, and by their advantages exhibited in a variety of applications [4–13].

Airy beams are the productions under the paraxial condition. They cannot propagate along bending paths of large curvatures [14,15]. As such, non-paraxial regime is explored to seek the solution to this problem. Half-Bessel accelerating beams became the first type to break the bending limitation [14]. A laser light shaped in a half Bessel profile can even turn to 90 degrees along a circular trajectory. Soon after the advent of the non-paraxial accelerating beam (NAB), it was found that properly shaped beams were also able to follow parabolic or elliptic paths [16–18]. Similar to the half-Bessel case, their beam profiles were obtained by using separation of variables to solve the Helmholtz equation. Thanks to the sharp bending effect, NABs are capable of delivering tiny particles to steeper angles that are not accessible for Airy beams in optical manipulation [19]. Further studies showed that the NABs can be designed to follow arbitrary convex paths [20,21]. Although various types of NABs were proposed, most work focused on a two-dimensional (2D) geometry (i.e., one transverse plus one propagation axis), leaving the beam patterns invariant in the orthogonal transverse direction [22–24]. Thus the resulting NABs were not able to reach a high peak intensity due to the loosen focusing. To overcome this drawback, one has to consider the design in the full space. Along this line, three-dimensional (3D) NABs moving along an arc were theoretically demonstrated [18,25]. In parallel, Bessel-like beams were also designed to follow trajectories of large curvatures [26]. However, to our knowledge, the

theoretical predictions on the 3D NABs have not been verified in experiment. Thus far, all the NABs observed experimentally have rather simple intensity patterns, distributed either in a 2D configuration or in a circular symmetry [27]. To generate the 3D NABs featured with complex profiles, there are two difficulties that one needs to overcome. Firstly, an additional amplitude modulation is generally required. This increases the experimental complexity comparing to the 2D case where only phase modulations are routinely employed. Secondly, an objective of a high numerical aperture is commonly used to reach a non-paraxial environment, but meanwhile it is likely to introduce sphere aberrations that tend to deviate the beam from the ideal path. Fortunately, this kind of aberration can be actively compensated. In such corrected system, the possibility to generate NABs with simple patterns has been demonstrated [28], but it is still a challenge to produce true 3D NABs having complex shapes. Here, we generate 3D NABs in an aberration compensation system. Both the phase and amplitude modulations for producing the beam are encoded in a phase-only pattern, and they are further combined with the correction phase needed for the aberration compensation. The accelerating solutions along an arc in parabolic, prolate spheroidal and oblate spheroidal coordinates are experimentally realized. Our observations are well reproduced in simulations.

2. Experimental method

The experimental setup is shown in Fig. 1(a). A Helium-Neon laser is expanded and collimated to illuminate a programmable phase-only spatial light modulator (SLM), where a proper phase modulation is imposed. The power of the light illuminating the SLM is 87.5 µW. Then the modulated light passes through a 4f system (consisting of a couple of conjugated lenses and a filter between them) and is further Fourier-transformed by an objective (i.e., O_1). The SLM is properly tilted to let the first order diffracted beam propagate along the optical axis defined by the objective. A microscope (consisting of another objective O_2 and a CCD) set on a motorized translation stage is employed to record the resulting beam pattern. The beam propagation profile is obtained by taking and stacking the captured snapshots at different locations.
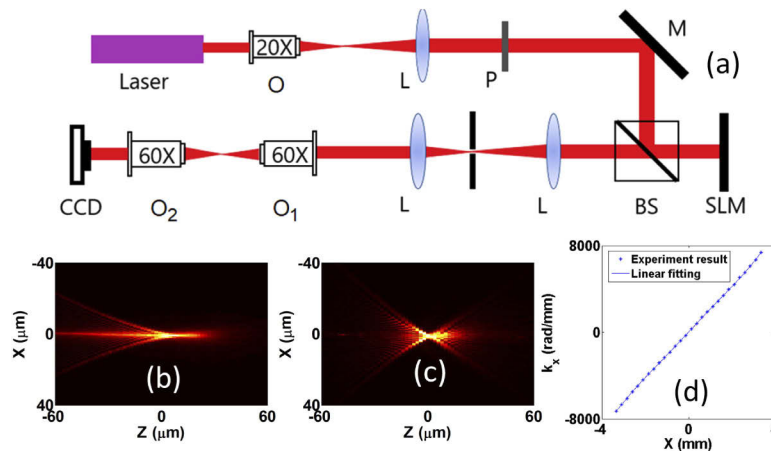

Fig. 1. (a) Schematic experimental setup for NABs. L: lens; BS: beam splitter; O: objective; P: polarizer; M: mirror; CCD: charge coupled device; (b) and (c) Experimentally obtained beam focusing via the objective O_1 when the aberration compensation is (b) off and (c) on; (d) measured relationship between the position on the SLM and the spatial frequency k_x.

In general, a spherical aberration exists for an objective working in a non-ideal condition. Since the objective we used is not designed for the beam propagation in air, which is the common case for most objectives, the beam cannot perform a good focusing in our system, as shown in

Fig. 1(b). This aberration is detrimental to the performance of a Fourier transformation that is necessary for generating the accelerating beams, considering that the NABs are theoretically designed in the momentum space. One can use the SLM to compensate it. By switching on a phase pattern carefully designed via the method proposed in [28], the beam can then be well focused [Fig. 1(c)]. To examine the performance of the Fourier transformation in such an aberration-compensated system, a small part (occupying 30×30 pixels on the SLM) of the input beam is selected to pass through the filter in the 4f system, while the remaining part is blocked. The unblocked part shows a collimated propagation after the objective O_1 and its tilt relative to the optical axis is employed to estimate its transverse wave vectors, i.e., k_x and k_y. By means of this examination for the small parts in different locations, we verify that our system builds a linear relationship between the position on the SLM and the transverse wave vector, as typically shown for the direction of k_x [Fig. 1(d)], thus meeting the condition of a Fourier transformation.

For all the 3D NABs to be studied in the following, amplitude modulations are necessary. Since the efficiency of the first order diffraction is influenced by the depth of the phase modulation, even a phase-only SLM can introduce an amplitude modulation following the method in [29]. Thus, in our experiment, the phase pattern imposed on the SLM combines the information for the phase and amplitude modulations associated with the NABs and that for the aberration correction phase.

3. Results

In the scalar case, the beam propagation under the non-paraxial condition can be described by the following formula [25]:

$$\Psi(\boldsymbol{r}) = \int_0^\pi \sin\theta \mathrm{d}\theta \int_{-\pi/2}^{\pi/2} \mathrm{d}\phi g(\theta) \exp(im\phi) \exp(ik\boldsymbol{r} \cdot \boldsymbol{u}) \tag{1}$$

where θ and ϕ are two angles defined in a spherical coordinate with a relation to the wave vector k_x, k_y, k_z by $\phi = \arctan(k_y / k_z)$, $\theta = \arctan(k_z / k)$ and $k^2 = k_x^2 + k_y^2 + k_z^2$, m is a positive real value, $\boldsymbol{u} = (\sin\theta\sin\phi, \cos\theta, \sin\theta\cos\phi)$, and $\boldsymbol{r} = (X, Y, Z)$ is the position in real space. Considering the symmetry of the spherical coordinate, any form of the function $g(\theta)$ is associated with an NAB following a circular path. The radius of trajectory is slightly larger than m/k. Thus one can simply control the radius for an NAB by changing the value of m. In our experiment, m is adopted as 1000 as a typical example, and the function $g(\theta)$ is considered in the framework of parabolic, prolate spheroidal and oblate spheroidal coordinate systems. The numerical beam propagation is readily obtained via simulating Eq. (1), where the associated integral is calculated by using the Fast Fourier Transform algorithm.

We start with the generation of NABs in a parabolic coordinate system. The spectral function of these beams can be written as:

$$g_\beta(\theta) = (\tan\theta/2)^{i\beta}/(2\pi\sin\theta) \tag{2}$$

where β is a constant. The associated caustics form an "X" shape as typically shown in Figs. 2(a) and 2(b). They are portions of two crossed parabolas with opposite opening directions parallel and antiparallel to Y-axis, and the location of their crossing point does not shift along X-axis as the value of β changes [25]. The resulting accelerating beams exhibit a pattern similar to the 2D Airy beams. Their main lobe locates at the crossing point of the caustics and the sub-lobes distribute towards left. During propagation, these beams follow a path of a half circle. Figure 2(c) shows the beam propagation associated with the case in Fig. 2(a) in the longitudinal section. For the case of other values of β, the beam paths have the same projection in X-Z plane, but experience a translation along Y axis. Employing the experimental parameters, we performed

numerical simulations as summarized in Figs. 2(d)–2(f), which have a good agreement with the measured results. The measured powers of both accelerating beams for the cases of $\beta = 0$ and 100 are 0.680 µW.
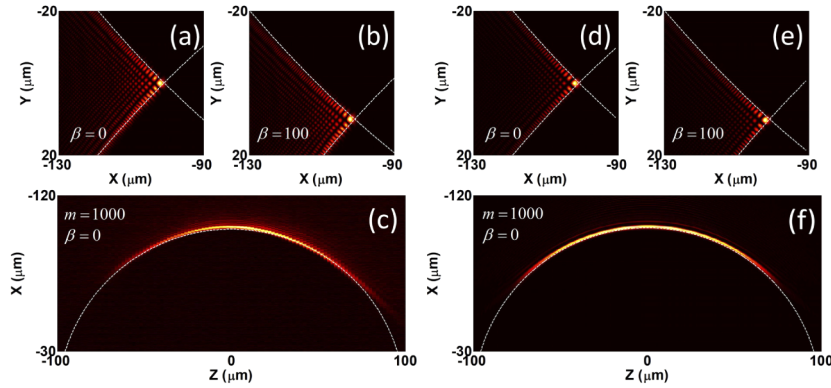

Fig. 2. Experimental results (a)-(c) and numerical simulations (d)-(f) of *parabolic* accelerating beams for different values of β. (a) and (b) Intensity profiles at $Z = 0$ plane; (c) propagation of the beam in (a); (d)-(f) correspond to (a)-(c). The white dashed lines depict the caustics.

A similar method is used to study the prolate spheroidal accelerating beams, the corresponding spectral function is

$$g_n^m(\theta; \gamma) = S_{m+n}^m(\cos \theta, \gamma) \tag{3}$$

where S_{m+n}^m is called as "spheroidal harmonics" [30], n is a positive integer, and γ is defined as $\gamma \equiv kf$ with f being the focal length of the prolate spheroidal coordinate system. This function is numerically calculated via the method in [31], which is more accurate in the condition of large γ (here $\gamma = 150$ is adopted). There are 3 caustics associated with this kind of accelerating beams, as typically shown in Figs. 3(a) and 3(b). ps_1 and ps_3 originate from two hyperbolas, while ps_2 is a prolate elliptic curve [25]. They determine the upper, bottom and right boundaries of the beam. The number of the peaks is $n + 1$ along the line ps_2, where higher peak values appear near the upper and bottom boundaries, and lower ones in the middle. For each peak, there are corresponding sub-lobes damping towards left. As the value of n increases, the vertical spacing between the upper and bottom boundaries becomes larger. Along propagation, these beams exhibit an acceleration following a half circle [Fig. 3(c)]. By using the experimental parameters, our simulations [Figs. 3(d)–3(f)] reproduce the measured results. The measured powers of the accelerating beams for the cases of $n = 2$ and 5 are 0.090 µW and 0.136 µW, respectively.

Finally, we design the oblate spheroidal accelerating beams by simply letting $\gamma \equiv ikf$ in the prolate spectral function, i.e., Eq. (3). Their caustics have two types according to the value of n. For the inner-type, two caustics following different hyperbolic lines bend along the same direction without a crossing, and they define the left and right boundaries of the beam [Fig. 4(a)]. For the outer-type, two caustics are hyperbolic and elliptic curves that have two crossings [Fig. 4(b)]. The right boundary of the beam is determined by both caustics. The number of the peaks along the right bending caustic is $n + 1$. Both beams show a similar accelerating propagation. Figure 4(c) presents the case associated with Fig. 4(a) as a typical example. Again, our numerical simulations [Figs. 4(d)–4(f)] have a good agreement with the experimental results [Figs. 4(a)–4(c)]. The measured powers of the accelerating beams for the cases of $n = 0$ and 10 are 0.023 µW and 0.197 µW, respectively.
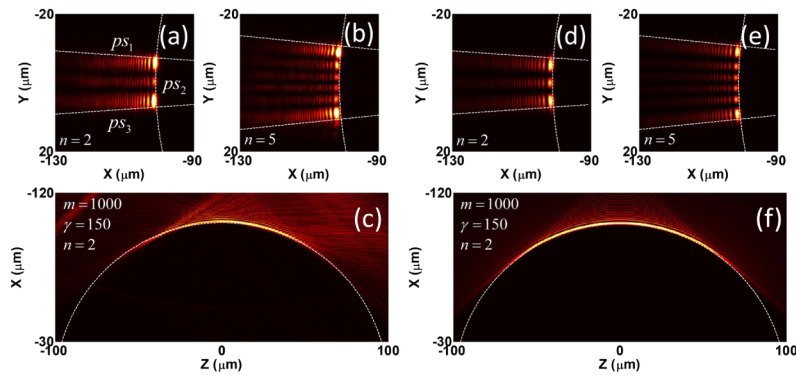
Fig. 3. Experimental results (a)-(c) and numerical simulations (d)-(f) of *prolate spheroidal* accelerating beams for different orders described by n. Other caption descriptions are the same with that in Fig. 2.
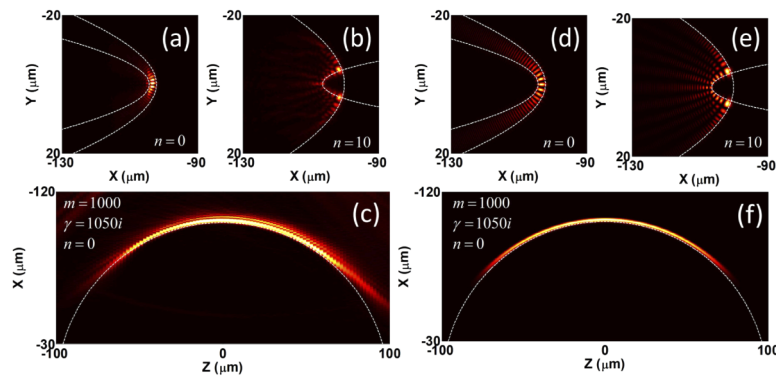

Fig. 4. Experimental results (a)-(c) and numerical simulations (d)-(f) of *oblate spheroidal* accelerating beams. $n = 0$ and 10 correspond to the outer- and inner-type, respectively. Other caption descriptions are the same with that in Fig. 2.

4. Conclusion

In conclusion, we have generated 3D NABs in an aberration compensated optical system. The shape-invariant solutions along an arc in parabolic, prolate spheroidal and oblate spheroidal coordinate systems are observed for the first time. The phase/amplitude modulation required for these beams and the phase for correcting the aberration are encoded in the same phase pattern. If a more compact setup is required for the purpose of integration and meanwhile dynamical tuning and controlling as the SLM performs are not concerned, one can instead resort to metasurfaces [13,32]. These accelerating beams can be used in optical tweezers for novel particle trapping and manipulation, and the associated beam shaping method may be adopted for generating other kinds of 3D beams in a microscale region.

Funding

Disclosures

The authors declare no conflicts of interest.

References

1. M. V. Berry and N. L. Balazs, "Nonspreading wave packets," Am. J. Phys. **47**(3), 264–267 (1979).
2. G. A. Siviloglou and D. N. Christodoulides, "Accelerating finite energy Airy beams," Opt. Lett. **32**(8), 979–981 (2007).
3. J. Broky, G. A. Siviloglou, A. Dogariu, and D. N. Christodoulides, "Observation of accelerating Airy beams," Phys. Rev. Lett. **99**(21), 213901 (2007).
4. J. Baumgartl, M. Mazilu, and K. Dholakia, "Optically mediated particle clearing using Airy wavepackets," Nat. Photonics **2**(11), 675–678 (2008).
5. T. Vettenburg, H. I. C. Dalgarno, J. Nylk, C. Coll-Lladó, D. E. K. Ferrier, T. Čižmár, F. J. Gunn-Moore, and K. Dholakia, "Light-sheet microscopy using an Airy beam," Nat. Methods **11**(5), 541–544 (2014).
6. P. Polynkin, M. Kolesik, J. V. Moloney, G. A. Siviloglou, and D. N. Christodoulides, "Curved plasma channel generation using ultraintense Airy beams," Science **324**(5924), 229–232 (2009).
7. J. X. Li, X. L. Fan, W. P. Zang, and J. G. Tian, "Vacuum electron acceleration driven by two crossed Airy beams," Opt. Lett. **36**(5), 648–650 (2011).
8. M. Clerici, Y. Hu, P. Lassonde, C. Milián, A. Couairon, D. N. Christodoulides, Z. Chen, L. Razzari, F. Vidal, F. Légaré, D. Faccio, and R. Morandotti, "Laser-assisted guiding of electric discharges around objects," Sci. Adv. **1**(5), e1400111 (2015).
9. T. Ellenbogen, N. Voloch-Bloch, A. Ganany-Padowicz, and A. Arie, "Nonlinear generation and manipulation of Airy beams," Nat. Photonics **3**(7), 395–398 (2009).
10. D. Abdollahpour, S. Suntsov, D. G. Papazoglou, and S. Tzortzakis, "Spatiotemporal Airy light bullets in the linear and nonlinear regimes," Phys. Rev. Lett. **105**(25), 253901 (2010).
11. C. Ament, P. Polynkin, and J. V. Moloney, "Supercontinuum generation with femtosecond self-healing Airy pulses," Phys. Rev. Lett. **107**(24), 243901 (2011).
12. Y. Hu, Z. Li, B. Wetzel, R. Morandotti, Z. Chen, and J. Xu, "Cherenkov Radiation Control via Self-accelerating Wave-packets," Sci. Rep. **7**(1), 8695 (2017).
13. M. Henstridge, C. Pfeiffer, D. Wang, A. Boltasseva, V. M. Shalaev, A. Grbic, and R. Merlin, "Synchrotron radiation from an accelerating light pulse," Science **362**(6413), 439–442 (2018).
14. I. Kaminer, R. Bekenstein, J. Nemirovsky, and M. Segev, "Nondiffracting accelerating wave packets of Maxwell's equations," Phys. Rev. Lett. **108**(16), 163901 (2012).
15. F. Courvoisier, A. Mathis, L. Froehly, R. Giust, L. Furfaro, P. A. Lacourt, M. Jacquot, and J. M. Dudley, "Sending femtosecond pulses in circles: highly nonparaxial accelerating beams," Opt. Lett. **37**(10), 1736–1738 (2012).
16. M. A. Bandres and B. M. Rodríguez-Lara, "Nondiffracting accelerating waves: Weber waves and parabolic momentum," New J. Phys. **15**(1), 013054 (2013).
17. P. Zhang, Y. Hu, T. Li, D. Cannan, X. Yin, R. Morandotti, Z. Chen, and X. Zhang, "Nonparaxial Mathieu and Weber accelerating beams," Phys. Rev. Lett. **109**(19), 193901 (2012).
18. P. Aleahmad, M. A. Miri, M. S. Mills, I. Kaminer, M. Segev, and D. N. Christodoulides, "Fully vectorial accelerating diffraction-free Helmholtz beams," Phys. Rev. Lett. **109**(20), 203902 (2012).
19. R. Schley, I. Kaminer, E. Greenfield, R. Bekenstein, Y. Lumer, and M. Segev, "Loss-proof self-accelerating beams and their use in non-paraxial manipulation of particles' trajectories," Nat. Commun. **5**(1), 5189 (2014).
20. A. Mathis, F. Courvoisier, R. Giust, L. Furfaro, M. Jacquot, L. Froehly, and J. M. Dudley, "Arbitrary nonparaxial accelerating periodic beams and spherical shaping of light," Opt. Lett. **38**(13), 2218–2220 (2013).
21. Y. Hu, D. Bongiovanni, Z. Chen, and R. Morandotti, "Multipath multicomponent self-accelerating beams through spectrum-engineered position mapping," Phys. Rev. A **88**(4), 043809 (2013).
22. Y. Yang, S. Yan, X. Yu, M. Li, and B. Yao, "Accelerating incoherent hollow beams beyond the paraxial regime," Opt. Express **24**(24), 27683–27690 (2016).
23. Y. Lumer, Y. Liang, R. Schley, I. Kaminer, E. Greenfield, D. Song, X. Zhang, J. Xu, Z. Chen, and M. Segev, "Incoherent self-accelerating beams," Optica **2**(10), 886–892 (2015).
24. Y. Zhang, H. Zhong, M. R. Belić, C. Li, Z. Zhang, F. Wen, Y. Zhang, and M. Xiao, "Fractional nonparaxial accelerating Talbot effect," Opt. Lett. **41**(14), 3273–3276 (2016).
25. M. A. Bandres, M. A. Alonso, I. Kaminer, and M. Segev, "Three-dimensional accelerating electromagnetic waves," Opt. Express **21**(12), 13917–13929 (2013).
26. I. D. Chremmos and N. K. Efremidis, "Nonparaxial accelerating Bessel-like beams," Phys. Rev. A **88**(6), 063816 (2013).
27. R. S. Penciu, Y. Qiu, M. Goutsoulas, X. Sun, Y. Hu, J. Xu, Z. Chen, and N. K. Efremidis, "Observation of microscale nonparaxial optical bottle beams," Opt. Lett. **43**(16), 3878–3881 (2018).
28. Y. Qiu, X. Mu, C. Zhang, X. Sun, Y. Hu, Z. Chen, and J. Xu, "Generation of non-paraxial accelerating beams by active aberration compensation," Opt. Commun. **437**, 11–16 (2019).
29. J. A. Davis, D. M. Cottrell, J. Campos, M. J. Yzuel, and I. Moreno, "Encoding amplitude information onto phase-only filters," Appl. Opt. **38**(23), 5004–5013 (1999).

30. A. Fletcher, "Spheroidal Wave Functions by C. Flammer," Math. Gaz. **43**(345), 217–218 (1959).
31. D. B. Hodge, "Eigenvalues and Eigenfunctions of the Spheroidal Wave Equation," J. Math. Phys. **11**(8), 2308–2312 (1970).
32. M. Henstridge, C. Pfeiffer, D. Wang, A. Boltasseva, V. M. Shalaev, A. Grbic, and R. Merlin, "Accelerating light with metasurfaces," Optica **5**(6), 678–681 (2018).